THE JOURNAL OF PHYSICAL CHEMISTRY C

Article

pubs.acs.org/JPCC

Ab Initio Molecular Dynamics Simulations of Nitrogen/VN(001) Surface Reactions: Vacancy-Catalyzed N_2 Dissociative Chemisorption, N Adatom Migration, and N_2 Desorption

D. G. Sangiovanni,*[,†] A. B. Mei,[‡] L. Hultman,[†] V. Chirita,[†] I. Petrov,[†,‡] and J. E. Greene[†,‡]

[†]Thin Film Physics Division, Department of Physics, Chemistry, and Biology (IFM), Linköping University, SE-58183 Linköping, Sweden

[‡]Departments of Materials Science, Physics, and the Frederick Seitz Materials Research Laboratory, University of Illinois, Urbana, Illinois 61801, United States

ABSTRACT: We use density-functional ab initio molecular dynamics to investigate the kinetics of N/VN(001) surface reactions at temperatures ranging from 1600 to 2300 K. N adatoms (N_{ad}) on VN(001) favor epitaxial atop-V positions and diffuse among them by transiting through 4-fold hollow (FFH) sites, at which they are surrounded by two V and two N surface atoms. After several atop-V → FFH → atop-V jumps, isolated N adatoms bond strongly with an underlying N surface (N_{surf}) atom. Frequent N_{ad}/N_{surf} pair exchange reactions lead to N_2 desorption, which results in the formation of an anion surface vacancy. N vacancies rapidly migrate via in-plane ⟨110⟩ jumps and act as efficient catalysts for the dissociative chemisorption of incident N_2 molecules. During exposure of VN(001) to incident atomic N gas atoms, N_{ad}/N_{ad} recombination and desorption is never observed, despite a continuously high N monomer surface coverage. Instead, N_2 desorption is always initiated by a N adatom removing a N surface atom or by energetic N gas atoms colliding with N_{ad} or N_{surf} atoms. Similarities and differences between N/VN(001) vs. previous N/TiN(001) results, discussed on the basis of temperature-dependent ab initio electronic structures and chemical bonding, provide insights for controlling the reactivity of NaCl-structure transition-metal nitride (001) surfaces via electron-concentration tuning.

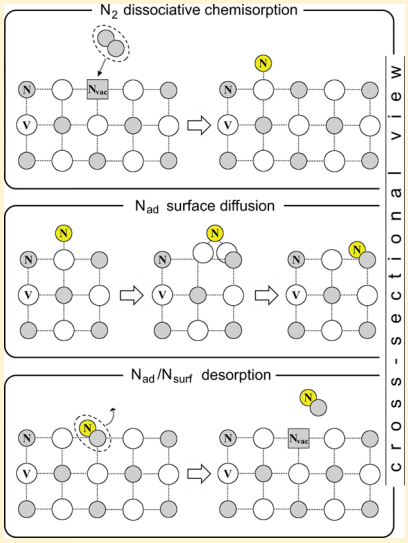

1. INTRODUCTION

Transition-metal (TM) nitride refractory compounds possess a unique combination of properties including high hardness,[1−3] toughness,[4,5] chemical inertness,[6,7] tunable optical properties,[8−10] thermal stability,[11] and good electrical conductivity.[2,12] Currently, these materials are widely employed as wear-resistant protective coatings on cutting tools[13] and engine components,[14] diffusion barrier in microelectronic devices,[15−18] and active layers in energy-harvesting thermoelectric and piezoelectric devices.[19,20] Recently, refractory TM nitrides have been suggested as highly promising candidates to replace noble metals in plasmonic devices for high-temperature optoelectronic applications.[21−23] In addition, they are known to exhibit high catalytic activities for important reactions including hydrogenolysis, hydrogenation, and methanation.[24−27]

The properties of TM nitrides ultimately depend on their nanostructure[28−32] and stoichiometry.[33−35] Growth and surface morphological evolution of titanium nitride (TiN), one of the first hard-coating materials,[36,37] have been extensively studied experimentally.[38−45] Vanadium nitride (VN), another important TM nitride, although not as well characterized as TiN, is of interest for low-friction, hard coatings.[46,47] Moreover, supercapacitors based upon VN deliver remarkable specific capacitance with high energy and high power densities, the properties required for developing efficient energy-storage devices.[48] VN and VN-based nanostructures are also promising anode materials for rechargeable lithium batteries.[49,50] Recently, NaCl-structure (cubic-B1) VN(001) has been identified as a novel electrode material for the synthesis of ammonia at room temperature and atmospheric pressure, a requirement for sustainable production of inorganic fertilizers.[51,52]

Understanding fundamental processes such as dissociative N_2 chemisorption, mass transport of N and metal adatoms, and associative N_2 desorption, which together control the nucleation and growth kinetics of TM nitride layers, requires resolving surface dynamics at the picosecond time scale. This is beyond the capabilities of atomic-scale experimental techniques such as scanning tunneling microscopy (STM)[38,39] and low-energy electron microscopy.[53] Thus, complementary computational investigations are necessary for detailed interpretation of experimental observations.

Received: March 14, 2016
Revised: May 18, 2016
Published: May 19, 2016

DOI: 10.1021/acs.jpcc.6b02652
J. Phys. Chem. C 2016, 120, 12503−12516

Ab initio density-functional theory (DFT) is routinely used to predict adatom and admolecule adsorption-energy landscapes, minimum energy paths, and migration energies E_a on surfaces at 0 K.[54−57] Diffusion rates can then be extrapolated to finite temperatures by transition-state theory[58,59] employing 0 K energy barriers and Arrhenius prefactors. This approximation, however, is not applicable to materials systems, such as NaCl-structure VN,[60] which is stable at room temperature due to large vibrational entropy contributions to the Gibbs free energy of formation but dynamically unstable with imaginary phonon frequencies at 0 K.[61] Molecular dynamics (MD) inherently resolves the above issues by integrating Newton's equations of motion for each atom. Thus, MD provides reliable diffusion rates and can reveal nonintuitive system configurations and reaction pathways at finite temperatures.[62,63]

Very few theoretical studies have considered the interaction of TM nitride surfaces with gases and metal adatoms via ab initio molecular dynamics (AIMD).[64,65] Recently, we investigated mass transport of Ti and N adatoms, together with TiN_x (x = 1−3) admolecules, on TiN(001)[62,66−69] and TiN(111)[70] surfaces and bulk diffusion in TiN[63] by both ab initio and classical molecular dynamics. MD simulations show that isolated N adatoms (N_{ad}) on TiN(001) favor 3-fold sites (TFS) near and strongly bonded with nitrogen surface atoms (N_{surf}) and bounded by two Ti surface atoms. After several N_{ad}/N_{surf} exchange reactions, over times corresponding to very few N_{ad} surface jumps, the N_{ad}/N_{surf} pair desorbs, thus leaving a N_{surf} vacancy in the upper substrate layer.[62]

Similar to our observations for N adatom behavior on TiN(001),[62] previous ab initio and experimental results indicate that oxygen adatoms on Group-IVb TM carbide (001) surfaces also adsorb in TFS positions and then desorb as CO molecules by extracting a carbon surface atom.[71−76] In contrast, DFT results,[72,73,77−79] supported by experimental observations,[76,80] show that oxygen monomers on (001) Group-IVb and Group-Vb TM nitride surfaces as well as Group-Vb and Group-VIb TM carbide surfaces are found to chemisorb close to *both* TFS and metal-atom atop sites with no distinct preference. For the pseudobinary $Ti_{0.5}Al_{0.5}N(001)$ surface, which has a valence electron concentration (VEC) of 8.5 (less than that of TiN and VC, both with VEC = 9), AIMD simulations[64] and X-ray photoelectron spectroscopy[81] results have shown that oxygen adatoms bond preferentially to metal surface atoms.

The experimental and theoretical observations described above suggest that the *e*lectron *c*oncentration in the vicinity of the *a*datom-adsorption-site (ECAS = substrate VEC + adatom valence-electron number) controls the behavior of isolated nonmetal adatoms on (001) TM nitride and carbide surfaces. For ECAS ≤ 14 (e.g., N_{ad} on the Group-IVb TM nitride TiN with ECAS = 14), nonmetal adatoms adsorb at TFS positions, strongly bonded to the nearest-neighbor nonmetal surface atom. In contrast, with ECAS > 14 (e.g., N_{ad} on the Group-Vb TM nitride VN with ECAS = 15), the adsorption energies for nonmetal adatoms residing close to either the cation or the anion surface site are comparable.

The population of surface electronic states affects not only preferred adatom adsorption sites but also the nature (attractive or repulsive) of adsorbate/adsorbate interactions.[82−87] For N adatoms on TiN(001), electronic-structure analyses show that associative N_{ad}/N_{ad} recombination and desorption is considerably less likely than N_{ad}/N_{surf} desorption due to the high activation energy (∼2 eV) required to overcome long-range N_{ad}/N_{ad} repulsive interactions.[62]

NaCl-structure TM nitride systems have wide single-phase compound fields, and varying the stoichiometry ratio (N/TM) during synthesis has been used to tune electrical,[34,88,89] optical,[90−92] structural,[93−96] catalytic,[97,98] and mechanical[33,35,89,99] properties. Thus, elucidation of the mechanisms leading to anion-vacancy formation and N_2 desorption during synthesis may provide guidance for adjusting experimental conditions to tailor the material's characteristics to meet specific requirements. Motivated by the outstanding properties of VN, we choose N_{ad}/VN(001), with ECAS = 15, as a model system to probe N_{ad} surface kinetics and compare the results with the previously reported behavior of N_{ad}/TiN(001),[62] ECAS = 14. We employ density-functional-based AIMD simulations to follow the dynamics of nitrogen incorporation and surface migration on, as well as desorption from, VN(001).

The paper is organized as follows. In section 2.1, we describe the methodology for calculating N/VN(001) surface dynamics and surface mass transport (including migration of isolated N adatoms and surface anion vacancies) as well as N_{ad}/N_{surf} exchange and desorption reaction rates from VN(001) as a function of temperature. A description of the model employed to simulate the interaction of N gas atoms with VN(001) is presented in section 2.2, while section 2.3 outlines the procedure used to calculate temperature-dependent electronic structures and the bonding nature of N_{ad}/VN(001) vs. N_{ad}/TiN(001). Results are presented in section 3. Sections 3.1 and 3.2 focus on the dynamics of isolated N adatoms on VN(001) and the effects of temperature on adatom/surface electronic structures and bonding characteristics. Dynamic and kinetic results for N_{ad}/N_{surf} surface exchange reactions and desorption from VN(001) are presented in section 3.3. Section 3.4 describes results for N-vacancy migration and vacancy-catalyzed N_2 dissociative chemisorption. AIMD simulation results for N gas interactions with VN(001) are summarized in section 3.5. Section 3 ends with a discussion (section 3.6) of the implications of N/VN(001) reaction kinetics on the catalytic properties of VN(001) surfaces. Our overall findings are summarized in section 4.

2. THEORETICAL METHODS

DFT-based AIMD simulations are carried out using the VASP code[100] implemented with the generalized gradient approximation (GGA)[101] and the projector augmented wave method.[102] The calculations are performed within the canonical ensemble NVT, integrating the equations of motion at 1 fs time intervals and controlling temperature via the Nosè−Hoover thermostat. At each time step, the total energy is evaluated to an accuracy of 10^{-5} eV/atom using a plane-wave energy cutoff of 400 eV while sampling the Γ-point in the Brillouin zone. Thermally-induced electronic excitations are accounted for by employing k_BT electron-smearing energies. Visual molecular dynamics (VMD) software[103] is used to generate images and videos of the results.

2.1. N Adatom and Vacancy Dynamics on VN(001). N adatom diffusion pathways and jump rates are probed as a function of temperature on 3 × 3 VN(001) surface unit cells. The substrate consists of three layers for a total of 108 atoms. The lateral size of the simulation cell is sufficient to avoid adatom self-interactions as shown previously for N_{ad}/TiN(001).[62] During all runs, the bottom slab layer remains fixed. This does not affect the substrate temperature, which depends only on the atomic-motion translational degrees of freedom. The simulation boxes contain a 16.8 Å thick vacuum layer to

DOI: 10.1021/acs.jpcc.6b02652
J. Phys. Chem. C 2016, 120, 12503−12516

minimize the interaction between VN(001) surface slab replicas. The average in-plane V−N nearest-neighbor distance $d_{NN//}$ in the simulation slab is obtained as a function of temperature, accounting for the experimental NaCl-structure VN average thermal expansion coefficient, 9.7×10^{-6} K^{-1},[104] by rescaling the 0 K DFT $d_{NN//}$ value (2.06 Å). Rescaling $d_{NN//}$ as a function of temperature is necessary to avoid spurious substrate strain effects on adatom jump rates.[105] Prior to initiating each AIMD run, thermal oscillations in the adatom-free simulation slab are allowed to stabilize for 2 ps, a time interval sufficient to equilibrate the system.

On TiN(001), N adatoms migrate almost exclusively among stable TFS positions, crossing metastable FFH sites; atop-Ti sites are rarely sampled.[62] In contrast, N adatoms on VN(001), due to the compound having an additional valence electron, can reside in TFS as well as atop-V sites. In order to identify the preferred N_{ad} adsorption site, 4-fold hollow sites on VN(001) are chosen as adatom starting positions. The probabilities for N adatoms jumping from initial FFH sites to neighboring epitaxial positions (atop-V) vs. a 3-fold site are proportional to jump-rate ratios $k_{FFH\rightarrow atop\text{-}V}/k^*$ and $k_{FFH\rightarrow TFS}/k^*$, respectively, for which $k^* = (k_{FFH\rightarrow atop\text{-}V} + k_{FFH\rightarrow TFS})$.

Stoichiometric VN crystallizes in the B1 NaCl structure over the temperature range from 250 K[60] (VN is tetragonal at lower temperatures) to the decomposition temperature T_{dec} = 2450 K.[106−108] This allows us to employ high simulation temperatures and obtain well-converged rate constants. AIMD runs of 0.525, 0.3, 0.125, and 0.1 ns are performed at 1600, 1900, 2100, and 2300 K, respectively.

The rate k_X of thermally activated process X is obtained by dividing the number of events n_X occurring during the time t_X the system remains in configurations from which the event X can be initiated. Activation energies E_X and attempt frequencies A_X are obtained using a linear regression fit to the Arrhenius equation

$$\ln[k_X(T)] = \ln(A_X) - \frac{E_X}{k_B T} \tag{1}$$

for which k_B is the Boltzmann constant. Statistical uncertainties σ_k, σ_κ, σ_E, and σ_A in the values of k, $\ln(k)$, E_X, and A are obtained as described previously.[62] In brief, σ_E and σ_A correspond to the widths of the normal distributions in E_X and A obtained from linear interpolation of a large number of stochastically created $\{\ln[k(T_i)]\}$ data sets. Gaussian $\ln[k(T_i)]$ distributions are characterized by standard deviations σ_κ. The sensitivity of surface rate constants k_X to substrate thickness is assessed in preliminary benchmarking tests employing five-layer slabs comprised of 180 atoms. Three AIMD test runs, 20 ps each, are performed at 1900 K, and another three runs of 20 ps each are carried out at 2100 K. N_{ad} migration, surface anion-vacancy jump rates, and N_{ad}/N_{surf} exchange rates, which are obtained with reasonably small uncertainties σ_k, are in good agreement with the corresponding k_X values determined for three-layer slabs.

N adatom surface migration is ultimately limited by N_{ad}/N_{surf} desorption. Thus, the diffusion coefficient of isolated N adatoms is negligible. Anion surface vacancies formed by N_{ad}/N_{surf} desorption migrate in plane (intralayer diffusion) with diffusivities $D_{Nvac}(T_i)$ estimated at temperatures T_i as

$$D_{Nvac}(T_i) = k_{Nvac}(T_i)\cdot d^2_{NN//}(T_i)/2 \tag{2}$$

Uncertainties σ_D in diffusion coefficient values are proportional to those of vacancy jump rates. Thus, activation energies E'_a and diffusion prefactors D_0, with corresponding uncertainties σ'_E and σ'_A, can be obtained from interpolation of the $\{D(T_i) \pm \sigma_D(T_i)\}$ data set. This leads to a general expression for temperature-dependent diffusion coefficients

$$D(T)\cdot[\sigma_D(T)]^{\pm 1} = A'\cdot(\sigma'_A)^{\pm 1}\cdot\exp[-(E'_a \mp \sigma'_E/\sqrt{2})/(k_B T)] \tag{3}$$

2.2. VN(001) Exposure to Atomic N Gas. AIMD simulations are also used to study the interaction of gas-phase N atoms with the VN(001) surface (results described in section 3.5). A 20 ps simulation is carried out at 1900 K, integrating the equations of motion at 2 fs time steps. The VN(001) slab, comprised of three layers, each containing 64 atoms, is thermally equilibrated for 3 ps. Ten N gas (N_{gas}) atoms, with initial velocities assigned stochastically, based upon a 1900 K Maxwell−Boltzmann distribution, are placed at random initial positions in a 10 Å thick vacuum region beginning 5 Å above the surface. A static monolayer of 64 He atoms (with the He−He interatomic spacing set to $d_{NN//}$) is added in the upper part of the simulation box, at ∼2 Å from the [001] supercell replica, to prevent gas adsorption at the *frozen* bottom slab layer. Helium is chemically inert and allows for faster calculations compared to the use of noble gases possessing p valence electrons.

The ideal gas law provides an estimate of the nitrogen gas pressure to which the surface is exposed. The simulated nitrogen pressure, ∼10 MPa ($\sim 75 \times 10^3$ Torr), is several orders of magnitude larger than N_2 pressures typically used during reactive magnetron sputter deposition (≤20 mTorr)[109] while comparable to that employed for the synthesis of stoichiometric VN by nitridation of vanadium at temperatures ranging from 1400 to 2000 K[104,110] and for producing bulk cubic VN_x ($0.74 \le x \le 1$) samples by float-zone and zone-annealing techniques at 2300 K.[111] High nitrogen pressures allow us to follow, over feasible simulation times, N and N_2 gas/surface reactions (both N and N_2 species are present in the plasma during reactive sputter deposition[112]).

2.3. N_{ad}/VN(001) and N_{ad}/TiN(001) Room-Temperature Electronic Structures. N_{ad}/TM_{surf} bonding (TM_{surf} = surface transition-metal atom) is investigated for both VN(001) and TiN(001) directly via AIMD simulations at 300 K. Accounting for the effect of lattice vibrations on the VN(001) electronic structure is necessary due to the instability of cubic VN below 250 K.[60] The calculations are carried out for VN(001) and TiN(001) slabs, each comprised of five layers with 4 × 4 atoms per layer (80 atoms) and two N_{ad} species in specular atop-TM_{surf} positions below the bottom layer and above the upper slab layer; mirroring is used in order to cancel adatom-induced slab polarization.[113] Six vacuum layers separate slab replicas along [001].

Representative 300 K electronic properties are determined by averaging over DFT results obtained for 50 different AIMD *frozen* atomic configurations stochastically extracted from 400 AIMD steps, with the condition that the distance of both adatoms from the original epitaxial atop-TM_{surf} positions is shorter than 1/8 of the metal−N in-plane spacing. For these calculations, the Brillouin zone is integrated on 5 × 5 × 1 Γ-centered k-point grids. We determine temperature-dependent density of states (DOS) projected onto spherical harmonics centered at atomic positions, charge densities resolved within

DOI: 10.1021/acs.jpcc.6b02652
J. Phys. Chem. C 2016, 120, 12503−12516

energy intervals containing N_{ad}/TM_{surf} hybridized states, and energy-resolved N_{ad}/TM_{surf} overlap populations (OP)[114,115] which are a projection of the local DOS into bonding (positive OP values) and antibonding (negative OP values) states. The overlap integrals are set to ±1, for which the sign depends on the relative orientation of N_{ad} and TM_{surf} orbitals.

3. RESULTS AND DISCUSSION

3.1. N Adatom Surface Migration. Figure 1 provides plan- and side-view schematic illustrations of N adatom migration on VN(001). At temperatures between 1600 and 2300 K, the most probable migration path for N_{ad} species starting in VN(001) FFH sites is toward epitaxial atop-V positions. N adatoms travel among epitaxial sites (Figure 1a and 1e), passing through transition-state FFH positions (Figure 1b and 1f). During migration, the N adatom pulls the V surface atom (V_{surf}) to which it is most strongly bonded toward the FFH site and attracts the opposite V_{surf} nearest neighbor (Figure 1b and 1f). The V_{surf}–N_{ad}–V_{surf} transition state quickly evolves into a stable configuration; N_{ad} species can jump to an epitaxial atop-V site (including back to the previous one (Figure 1c and 1g)) or, more rarely, to one of the neighboring TFS positions (Figure 1d and 1h) with the two V_{surf} atoms returning to their initial positions.

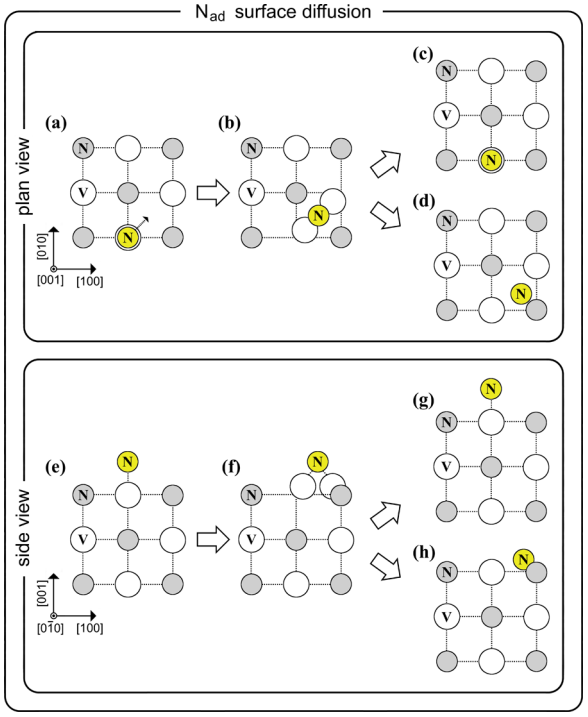

Figure 1. Schematic representation of $N_{ad}/VN(001)$ surface diffusion in (a–d) plan views and (e–h) side views. (a, e) Favored site for N_{ad} adsorption is the epitaxial atop-V position. (b, f) N_{ad} surface migration occurs via FFH transition states. From a FFH site, N_{ad} can migrate to either (c, g) an atop-V site or (d, h) a TFS position, close to a N surface atom. FFH = 4-fold hollow and TFS = 3-fold site.

N_{ad} transition rates [atop-V → FFH] and [FFH → TFS] follow Arrhenius relationships over the temperature range investigated (see Figure 2). Between 1600 and 2300 K, $k_{atop\text{-}V\rightarrow FFH}$ values are one to 2 orders of magnitude larger than $k_{FFH\rightarrow TFS}$. Note, however, that $k_{FFH\rightarrow TFS}$ accounts only for the time spent by a nitrogen adatom in FFH positions (see section 2.1), which is a small fraction of the total surface-migration time. From the dependence of $\ln(k_{diff})$ on 1/T, we extract activation energies $E_{atop\text{-}V\rightarrow FFH} = 0.79 \pm 0.13$ eV and $E_{FFH\rightarrow TFS} = 1.5 \pm 0.9$ eV, with attempt frequencies $A_{atop\text{-}V\rightarrow FFH} = 4.82(x2.6^{\pm1})x10^{13}$ s^{-1} and $A_{FFH\rightarrow TFS} = 52(x60^{\pm1})x10^{13}$ s^{-1}. The large error bars for $k_{FFH\rightarrow TFS}$ rates are due to low statistics for these events.

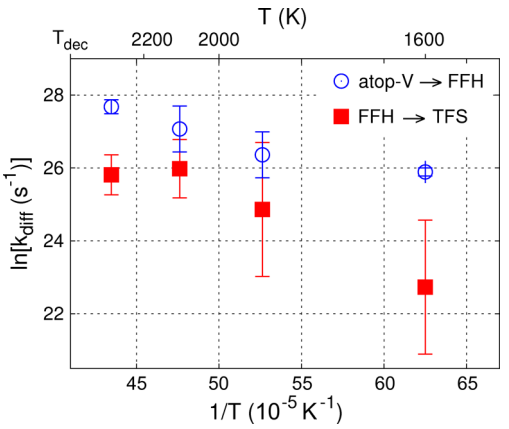

Figure 2. N_{ad} diffusion jump rate k_{diff} on VN(001) as a function of temperature T. Red filled squares correspond to adatom migration from FFH sites to TFS positions along ⟨110⟩ directions. Blue open circles correspond to the rate of ⟨110⟩ N_{ad} migration from atop-V to FFH. The VN decomposition temperature T_{dec} is ∼2450 K. FFH = 4-fold hollow and TFS = 3-fold site.

N_{ad} in a TFS position bonds strongly to the underlying nearest-neighbor N_{surf}; it is therefore unlikely that a free N monomer reforms (see section 3.3) after N_{ad} [FFH → TFS] migration. Thus, N adatom migration on VN(001) occurs preferentially along atop-V → FFH → atop-V pathways. In contrast, on TiN(001), N_{ad} species move almost exclusively among TFS, through FFH, by breaking and reforming highly energetic N_{ad}/N_{surf} bonds.[62] This results in significantly higher N_{ad} mobilities on VN(001) than on TiN(001) at all temperatures (Figure 3). Nevertheless, as described below, the N_{ad} surface mobility is ultimately limited for *both* VN(001) and TiN(001) by N_{ad}/N_{surf} desorption rates.

AIMD simulations at 1900 K also reveal an unexpected N_{ad}/VN(001) reaction. On one occasion, a N adatom pulls a V

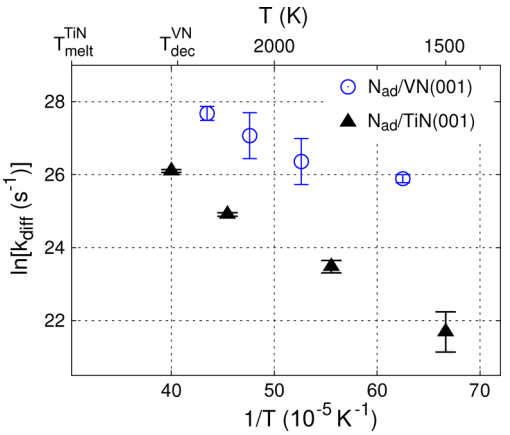

Figure 3. N_{ad}/VN(001), blue open circles, and N_{ad}/TiN(001), black filled triangles, jump rates k_{diff} as a function of temperature T. VN decomposition temperature T_{dec}^{VN} is ∼2450 K, and the TiN melting point T_{melt}^{TiN} is ∼3200 K.

DOI: 10.1021/acs.jpcc.6b02652
J. Phys. Chem. C 2016, 120, 12503–12516

surface atom onto the surface to form a VN admolecule while a second-layer V atom moves into the vacated upper-layer cation site, indicating relatively strong V−V bonds in VN.[116] After a few VN dimer rotations, the V dimer atom displaces a V surface atom which fills the second-layer cation vacancy. Rotation of TiN_x (x = 1−3) species was previously observed during classical molecular dynamics simulations of admolecule diffusion on TiN(001) terraces and islands.[67,69]

3.2. N_{ad}/VN(001) and N_{ad}/TiN(001) Electronic Structures. In section 1, we proposed an empirical rule based on adatom/surface electron densities, ECAS = substrate VEC + adatom valence-electron number, which systematizes in a consistent manner the present AIMD results, as well as previous experimental and ab initio results, for preferred nonmetal adatom adsorption sites on TM nitride and carbide (001) surfaces. In adsorption reactions for which ECAS is ≤14, nonmetal adatoms adsorb at TFS positions, strongly bonded to the nearest-neighbor nonmetal surface atom. However, with ECAS > 14, the adsorption energies for nonmetal adatoms residing close to either cation or anion surface sites are comparable (see literature survey in section 1).

On TiN(001), N adatoms adsorb and migrate exclusively among TSF positions[62] as both FFH and atop-Ti_{surf} sites are saddle points in the N_{ad}/TiN(001) adsorption-energy landscape,[117] consistent with an ECAS value of 14. In contrast, on VN(001) (ECAS = 15), N adatoms travel primarily among atop-V surface epitaxial sites, also in agreement with the empirical prediction, and the formation of N_{ad}/N_{surf} pairs is kinetically hindered.

Room-temperature electronic properties explain the role of the additional valence electron for VN(001) vs. TiN(001) in stabilizing N adatoms at surface epitaxial sites. Figures 4, 5, and 6 are plots of densities of states, overlap populations, and

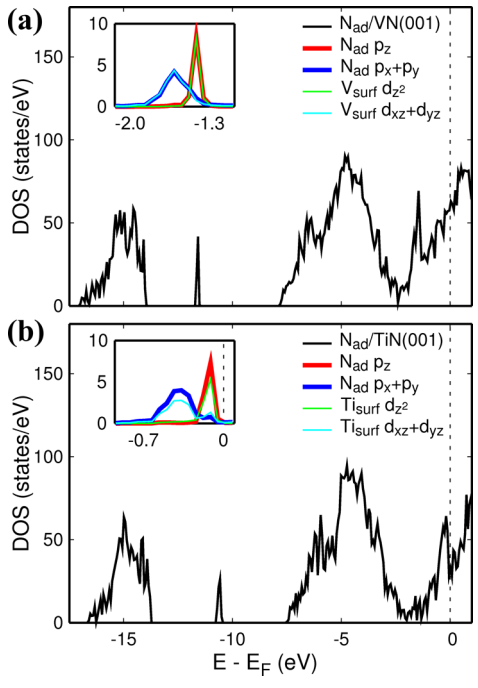

Figure 4. Density of states projected onto spherical harmonics centered at atomic positions for (a) VN(001) and (b) TiN(001) with a N adatom at an atop-TM_{surf} site at 300 K. (Insets) Enlarged views of N_{ad}/TM_{surf} hybridized states.

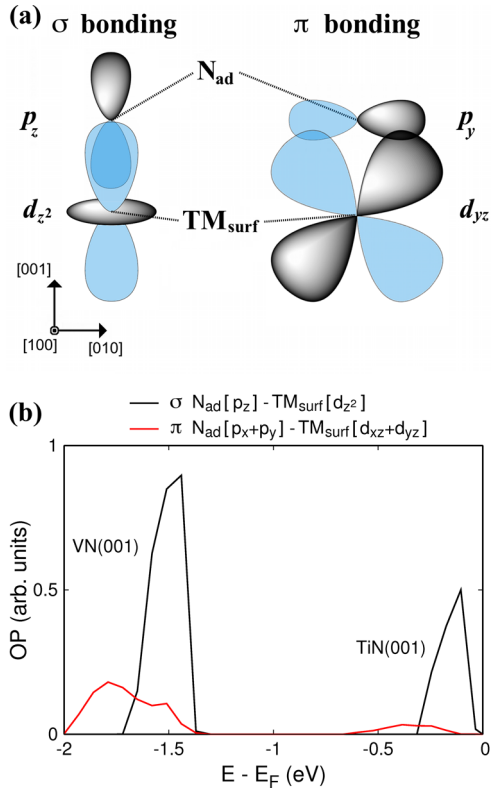

Figure 5. N_{ad}/TM_{surf} bonding on VN(001) and TiN(001). (a) Schematic representation of N_{ad}/TM_{surf} orbital overlap. (b) Overlap population (OP) for σ and π N_{ad}/TM_{surf} bonding states near the Fermi level.

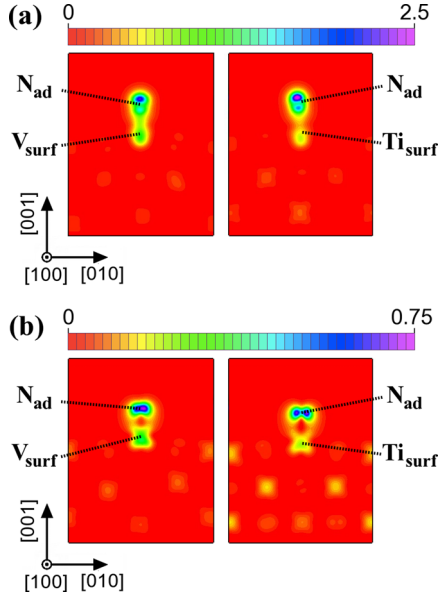

Figure 6. Energy-resolved charge densities for N adatoms at atop-TM_{surf} positions on TiN(001) and VN(001) at 300 K: (a) σ $N_{ad}(p_z)$−$TM_{surf}(d_z^2)$ and (b) π $N_{ad}(p_x + p_y)$−$TM_{surf}(d_{xz} + d_{yz})$ bonding states (see schematic orbital representations in Figure 5a). (a) Energy intervals used for σ bonding are from −1.7 to −1.3 eV for N_{ad}/VN(001) and from −0.3 to 0 eV for N_{ad}/TiN(001). (b) Energy intervals used for π bonding are from −2.0 to −1.7 eV for N_{ad}/VN(001) and from −0.7 to −0.3 eV for N_{ad}/TiN(001). Red to violet color scales are in units of electrons/Å^3.

DOI: 10.1021/acs.jpcc.6b02652
J. Phys. Chem. C 2016, 120, 12503−12516

electron densities in N_{ad}/TM_{surf} hybridized states for VN(001) and TiN(001) with a N adatom placed at atop-TM_{surf} positions.

DOS curves calculated for N_{ad}/VN(001) and N_{ad}/TiN(001) exhibit very similar shapes. However, due to VN having a higher electron density than TiN, the DOS of VN is shifted to lower energies. The sharp DOS peaks near the Fermi energies of N_{ad}/VN(001), Figure 4a, and N_{ad}/TiN(001), Figure 4b, derive mainly from σ $N_{ad}(p_z)-TM_{surf}(d_z^2)$ states. For VN, these states are located at binding energies which are ~1.3 eV higher than for TiN (see insets in Figure 4a and 4b). A secondary adatom/surface electronic interaction stems from π $N_{ad}(p_x + p_y)-TM_{surf}(d_{xz} + d_{yz})$ orbitals, centered at approximately −1.8 eV for VN and −0.4 eV for TiN.

For both VN(001) and TiN(001) surfaces, $(p_z)-(d_z^2)$ and $(p_x + p_y)-(d_{xz} + d_{yz})$ N_{ad}/TM_{surf} orbital overlap, schematically illustrated in Figure 5a, produce bonding σ and π states, respectively, as evidenced by the OP vs. energy curves in Figure 5b remaining positive. A comparison of the magnitude of N_{ad}/VN(001) vs. N_{ad}/TiN(001) OP values demonstrates that σ and π N_{ad}/TM_{surf} bonds are both much stronger for VN(001) (Figure 5b). The shift in adatom surface states to lower energies, together with N_{ad}/V_{surf} bonds being significantly stronger than N_{ad}/Ti_{surf} bonds, explains the gain in N adatom stability at epitaxial sites provided by the additional valence electron in VN.

The latter finding is supported by results for charge densities resolved within energy intervals containing primarily N_{ad}/TM_{surf} electronic states. While specific chemical bonds are not easily distinguishable in the total electron density of a solid, the partial charge density technique allows visualization of the chemical bond of interest. The energy intervals used to map N_{ad}/TM_{surf} bonds (see insets in Figure 4) range from −1.6 to −1.3 eV for σ bonds, from −2.0 to −1.6 eV for π bonds on VN(001), from −0.3 eV to the Fermi level for σ bonds, and from −0.7 to −0.3 eV for π bonds on TiN(001). The electron distributions in Figure 6 confirm that both σ and π N_{ad}/TM_{surf} bonds are much stronger for VN than for TiN due to higher electron densities between N_{ad} and V_{surf} atoms.

3.3. N_{ad}/N_{surf} Surface Exchange Reactions and Desorption. The bond strength and vibrational frequency of N_{ad}/N_{surf} pairs on VN(001) are similar to those of isolated N_2 gas molecules. The preferred bond-axis orientation of N_{ad}/N_{surf} pairs is along ⟨111⟩ but frequently changes from ⟨111⟩ to ⟨110⟩ to ⟨111⟩, resulting in N_2 dimer rotation. Analogous behavior was reported for N_{ad}/N_{surf} pairs on TiN(001),[62] as well as for N-interstitial/N-lattice dimers in bulk TiN and CrN.[63,118]

The most probable N_{ad}/N_{surf} rotation event on VN(001) is precession, with the N adatom migrating among TFS sites in adjacent surface unit cells while remaining anchored to the same N_{surf} atom, Figure 7a and 7b. Rotation can also occur by N_{ad}/N_{surf} exchange. In this case, N_{ad} takes the position of N_{surf} (Figure 7c), which is pushed upward into the diagonally opposite TFS position (Figure 7d). Calculated N_{ad}/N_{surf} exchange activation energies and attempt frequencies are E_{exch} = 0.46 ± 0.11 eV and A_{exch} = $2.26(\times 1.9^{\pm 1}) \times 10^{13}$ s^{-1}, respectively. On TiN(001), N_{ad}/N_{surf} exchange occurs less frequently, E_{exch} = 0.69 ± 0.09 eV and A_{exch} = $1.00(\times 1.7^{\pm 1}) \times 10^{13}$ s^{-1},[62] reflecting stronger metal−N bonds than for VN(001). Occasionally (three observations at 2300 K and two at 2100 K), N_{ad}/N_{surf} exchange on VN(001) provides sufficient kinetic energy for N_{surf} to break the N_{ad}/N_{surf} bond and move to a neighboring epitaxial position (Figure 7e) as a *free* N adatom. Exchange-induced N_{surf} jumps were also observed in AIMD simulations of N_{ad}/TiN(001) migration.[62] In the latter case, however, N_{surf} moves to a metastable TiN(001) FFH position.

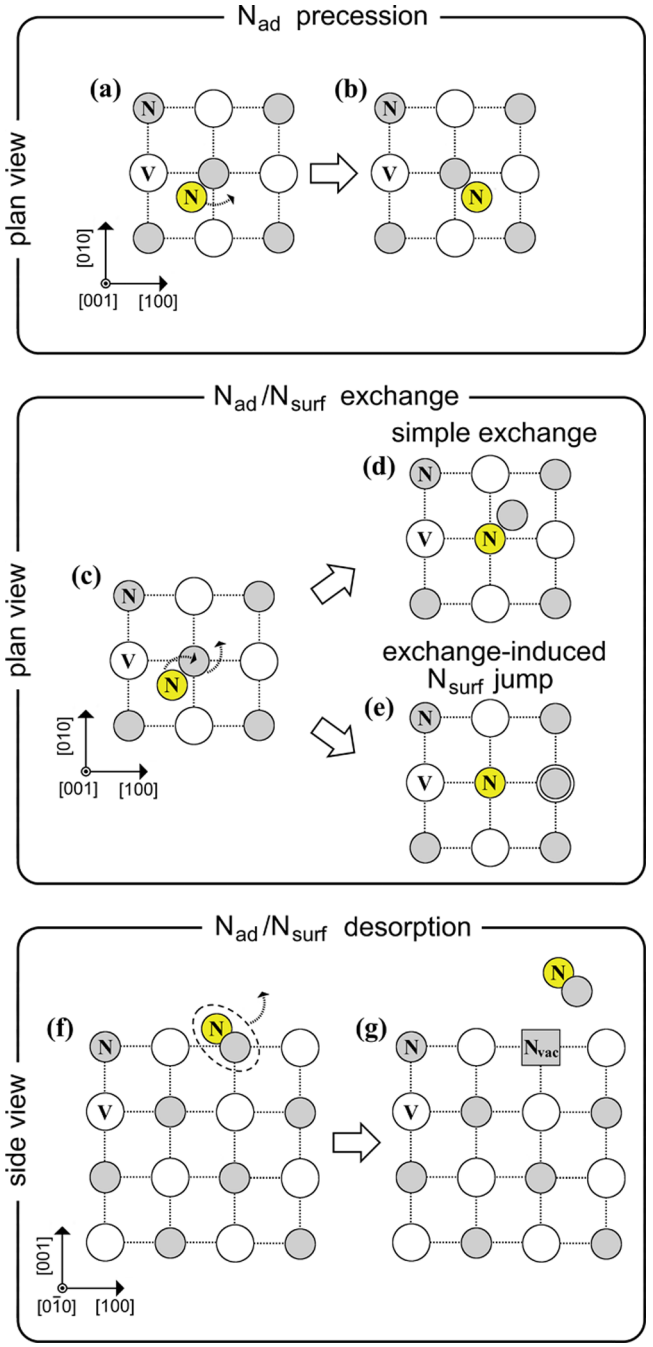

Figure 7. Schematic representation of VN(001) surface reactions initiated by N_{ad} adsorbed in TFS positions. (a, b) N adatom precession among TFS positions in adjacent surface unit cells. (c) Exchange of a N adatom with a N surface atom (in which N_{ad} takes the position of N_{surf}) can result in (d) simple exchange, with N_{surf} moving into the diagonally opposite TFS position, or (e) an exchange-induced N_{surf} jump, with N_{surf} moving onto the adjacent epitaxial atop site. (f) After several N_{ad}/N_{surf} exchange reactions, the N_{ad}/N_{surf}-pair desorbs, leaving (g) an anion surface vacancy (N_{vac}).

The most probable reaction, after several N_{ad}/N_{surf} exchange events, is N_{ad}/N_{surf} molecular desorption, Figure 7f, which results in the creation of an anion vacancy in the VN(001)

DOI: 10.1021/acs.jpcc.6b02652
J. Phys. Chem. C 2016, 120, 12503−12516

surface (Figure 7g). N_{ad}/N_{surf} desorption rates on VN(001), calculated considering only the time spent by N adatoms in TSF positions, correspond to attempt frequencies A_{des} = $3.51(\times 12^{\pm 1}) \times 10^{13}$ s^{-1} and activation energies E_{des} = 0.84 ± 0.40 eV (Figure 8). Even accounting for the time spent by N

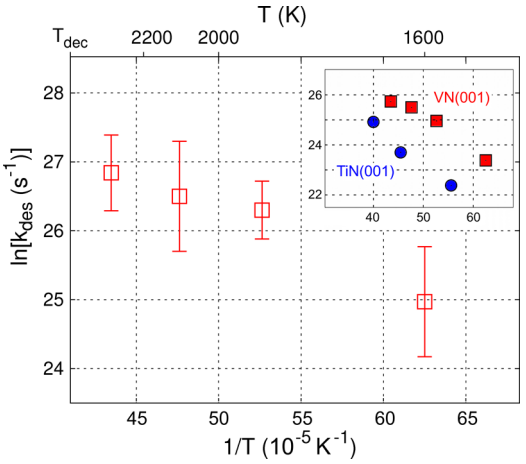

Figure 8. N_{ad}/N_{surf} desorption rates k_{des} from VN(001) as a function of temperature T. (Inset) Comparison of the N_{ad}/N_{surf} desorption rate from VN(001) to that from TiN(001) accounting for N_{ad} surface migration times among epitaxial sites prior to N_{ad}/N_{surf} bond formation.

adatoms in migrating among atop-V sites, which lowers N_{ad}/N_{surf} desorption rates, N_{ad}/N_{surf} desorption from VN(001) (A_{des} = $4.65(\times 12^{\pm 1}) \times 10^{13}$ s^{-1} and E_{des} = 1.00 ± 0.40 eV) is overall much more frequent than from TiN(001) (A_{des} = $3.37(\times 5^{\pm 1}) \times 10^{13}$ s^{-1} and E_{des} = 1.37 ± 0.30 eV)[62] (see inset in Figure 8).

The ratio $k_{diff}(T)/k_{des}(T)$ of N_{ad} diffusion rates k_{diff} to N_{ad}/N_{surf} desorption rates k_{des} quantifies N_{ad} mean surface migration events as a function of T (Figure 9). For TiN(001), $k_{diff}(T)/k_{des}(T)$ = $3.53 \cdot \exp[-0.02\ \text{eV}/(k_B T)]$, indicating that the average number of N_{ad} surface migration events prior to N_2 desorption is three or four, independent of T between room temperature[119] and the melting point. In contrast, $k_{diff}(T)/k_{des}(T)$ varies significantly with T for N_{ad} on VN(001): $k_{diff}(T)/k_{des}(T)$ = $0.96 \cdot \exp[0.21\ \text{eV}/(k_B T)]$. At 600 K, N_{ad} jumps among VN(001) epitaxial sites approximately 100 times prior to N_{ad}/N_{surf} desorption; for T approaching the VN decomposition temperature, 2450 K, the adatom performs very few jumps, ~3, before leaving the surface as a N_{ad}/N_{surf} molecule.

The fact that the kinetics of N_{ad} migration on, and N_{ad}/N_{surf} desorption from, VN(001) (ECAS = 15) approaches, with increasing temperatures, that observed for TiN(001) (ECAS = 14) is attributed to progressively stronger vibrational effects which effectively cancel out the atop-V stability gain derived from the additional valence electron. The $k_{diff}(T)/k_{des}(T)$ ratio results described above imply that, during (001) layer growth, the VN_x nitrogen fraction x is more sensitive to temperature than that of TiN_x. The fact that relatively low deposition temperatures delay N_2 desorption with respect to surface diffusion on VN(001) is consistent with experimental results for epitaxial layers grown by magnetron sputter deposition. High-quality single-crystal fully dense cubic VN(001) thin films have been synthesized at ~700 K.[109] For comparison, the

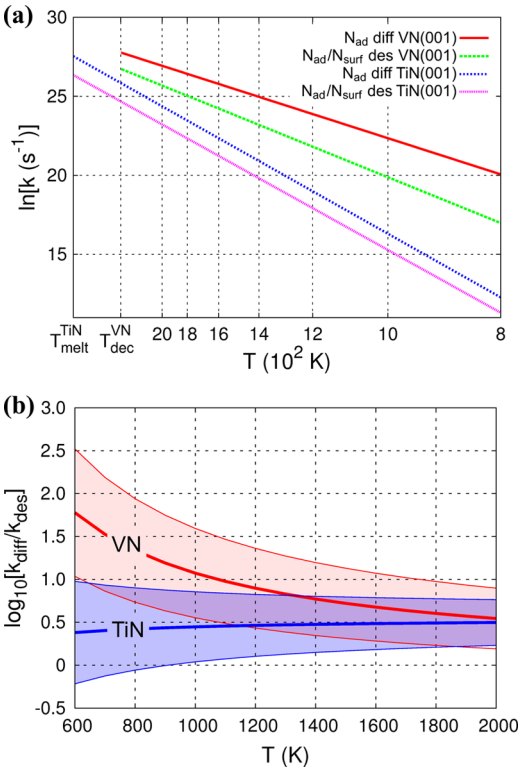

Figure 9. (a) Comparison of N_{ad} migration rates k_{diff} on and N_{ad}/N_{surf} desorption rates k_{des} from VN(001) and TiN(001) as a function of temperature T. (b) Temperature-dependent ratio of the N_{ad} migration rate to the N_{ad}/N_{surf} desorption rate for the two surfaces. Shaded areas indicate uncertainty ranges.

optimum temperature range for growth of dense epitaxial TiN(001) layers is ~1000−1200 K.[88,120]

Figure 10, summarizing the above-described surface reactions, illustrates a typical diffusion pathway for N_{ad} on VN(001) at 1600 K. Within a fraction of a picosecond, the adatom migrates from its starting FFH position, labeled as time t = 0, to

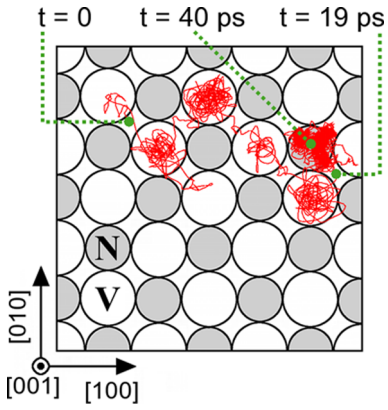

Figure 10. AIMD N_{ad} migration pathway (solid red line) during 40 ps on VN(001) at 1600 K. The N adatom is initiated (t = 0) at a FFH site. Between 0 and 19 ps, N_{ad} migrates among V-atop sites (six ⟨110⟩ diffusion events) by passing through FFH positions. At t = 19 ps, the adspecies jumps from a FFH to a TFS position, in which it bonds strongly to a N_{surf} atom. During the remaining 21 ps, 17 N_{ad}/N_{surf} exchange reactions are recorded. At t = 40 ps, the N_{ad}/N_{surf} pair desorbs, leaving a N surface vacancy. Color legend: V_{surf} = open circles, N_{surf} = gray filled circles.

DOI: 10.1021/acs.jpcc.6b02652
J. Phys. Chem. C 2016, 120, 12503−12516

a stable atop-V epitaxial site. The adatom trajectory during the initial 19 ps of the simulation reveals that N_{ad} spends relatively long times at atop-V epitaxial positions while moving rapidly through FFH sites. At t = 19 ps, following six atop-V → FFH → atop-V surface transitions, the N adatom migrates from a FFH to a TFS site, in which it remains as part of a N_{ad}/N_{surf} pair for an additional 21 ps. The N_{ad}/N_{surf} dimer exchanges positions 17 times before desorbing as N_2 at t = 40 ps.

3.4. N-Vacancy Surface Migration and Vacancy-Catalyzed N_2 Dissociative Chemisorption. N_{ad}/N_{surf} desorption results in the formation of nitrogen surface vacancies N_{vac} which give rise to relatively frequent N_{vac}/VN(001) intralayer migration events at all temperatures investigated (1600−2300 K). In contrast, N_{vac} intralayer migration was never observed in AIMD simulations of N_{vac}/TiN(001) dynamics at temperatures up to 2500 K[62] due to stronger metal−N bonds in TiN than in VN. N_{vac} surface migration requires one of the four neighboring N_{surf} atoms to migrate along ⟨110⟩ and fill the vacant anion site (Figure 11a).

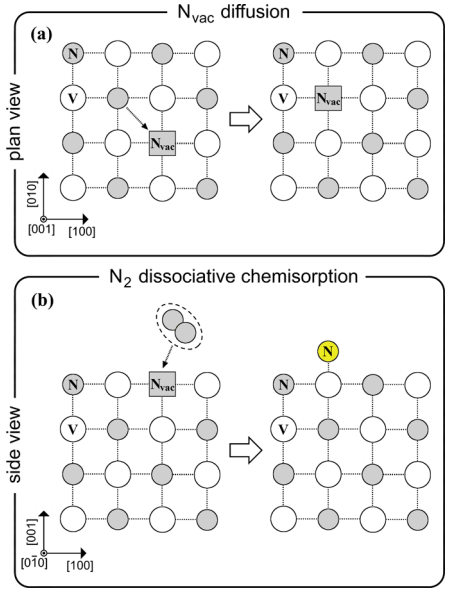

Figure 11. (a) N vacancy migration along ⟨110⟩ requires one of the four neighboring N_{surf} atoms to jump into the empty surface anion site. (b) During N_2 dissociative chemisorption at surface anion vacancies, one N atom fills the vacancy site while the other becomes a free adatom.

In-plane diffusion of isolated N vacancies occurs with attempt frequencies A_{Nvac} = 0.31(×1.4$^{\pm1}$) × 10^{13} s^{-1} and activation energies E_{Nvac} = 0.25 ± 0.05 eV (Figure 12), yielding diffusivities (eqs 2 and 3) with prefactors A'_{Nvac} = 7.25(×1.3$^{\pm1}$) × 10^{-4} cm^2 s^{-1} and activation energies E'_{Nvac} = 0.26 ± 0.03 eV.

N_{vac} interlayer diffusion in VN(001) is observed only once during a total simulation time of 40 ps and only at the highest temperature, 2300 K, as a second-layer N atom fills a vacant anion surface site. This indicates that anion surface vacancies are highly stable, as expected for all TM nitrides; strong TM−N bonds hinder N diffusion.[63,121]

Due to the use of periodic boundary conditions, desorbed N_{ad}/N_{surf} molecules rebound from the bottom layer of the overlying slab replica to return to the upper layer of the slab from which they desorbed. AIMD simulations show that the presence of N vacancies catalyzes N_2 molecular dissociation on

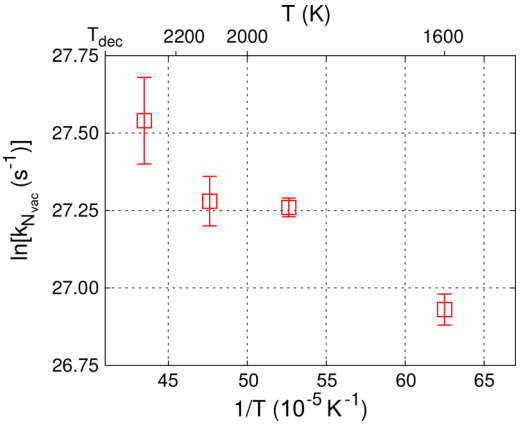

Figure 12. N_{vac}/VN(001) in-plane jump rate k_{Nvac} as a function of temperature T. N_{vac} is a N surface vacancy and T_{dec} ≈ 2450 K is the VN decomposition temperature.

VN(001), as observed previously for TiN(001).[62] N_2 dissociation is never observed for gas molecules incident at defect-free VN(001) surface regions. Occasionally, however, a N_2 molecule lands proximate to an anion surface vacancy. In each of these cases, one of the N_2 nitrogen atoms moves into the vacant anion site, while the other remains on the surface as a free adatom (Figure 11b). This is analogous to the mechanism proposed, based upon STM experiments, for O_2 dissociation on TiO_2(110).[122] AIMD movies also show that N_2 dissociation on VN(001) can be directly followed by a N_{ad}/N_{surf} desorption reaction promoted by momentum transfer to the surface from the incident gas molecule.

Overall, N_2 dissociative chemisorption on VN(001) occurs every time a N_2 molecule is incident at the surface within approximately one interatomic distance $d_{NN//}$ from an anion vacancy (five events in total), from which we infer that anion vacancies on NaCl-structure VN(001) are efficient catalytic agents.

3.5. N Gas Reactions on VN(001). In recent AIMD and DFT investigations we have shown that N_{ad}/N_{ad} recombination on, and subsequent desorption from, TiN(001) is much less likely than N_{ad}/N_{surf} desorption (E_{des} = 1.4 eV) due to N_{ad}/N_{ad} repulsive energies which rapidly increase to 2 eV as adatom/adatom separation decreases to 1.5 Å.[62] The probability of N_{ad}/N_{ad} recombination on TiN(001) is further reduced because of the extremely short average distances traveled by isolated N adatoms prior to N_{ad}/N_{surf} desorption.[62] The 0 K phonon instability of cubic VN[61] does not allow for quantification of adatom/adatom attractive/repulsive potential-energy pathways on VN(001) via DFT. Thus, we carry out AIMD simulations to probe the interaction of N gas atoms on VN(001) at 1900 K, well above 250 K, at which the cubic phase becomes stable,[60] in order to provide direct insight as to whether N_{ad}/N_{ad} recombination and desorption is more or less likely to occur than N_{ad}/N_{surf} pair formation and desorption (see section 2.2 for computational details).

Figure 13 shows four images extracted from N_{gas}/VN(001) AIMD movies. Due to the complexity of N_{gas}/VN(001) reactions, it is difficult to accurately determine the fraction of incident N gas atoms reflected from the surface. We estimate that there are one or two N_{gas} reflections out of a total of approximately 40 N_{gas}/VN(001) surface collisions, yielding a capture probability of ∼97%. N gas atoms are adsorbed on

DOI: 10.1021/acs.jpcc.6b02652
J. Phys. Chem. C 2016, 120, 12503−12516

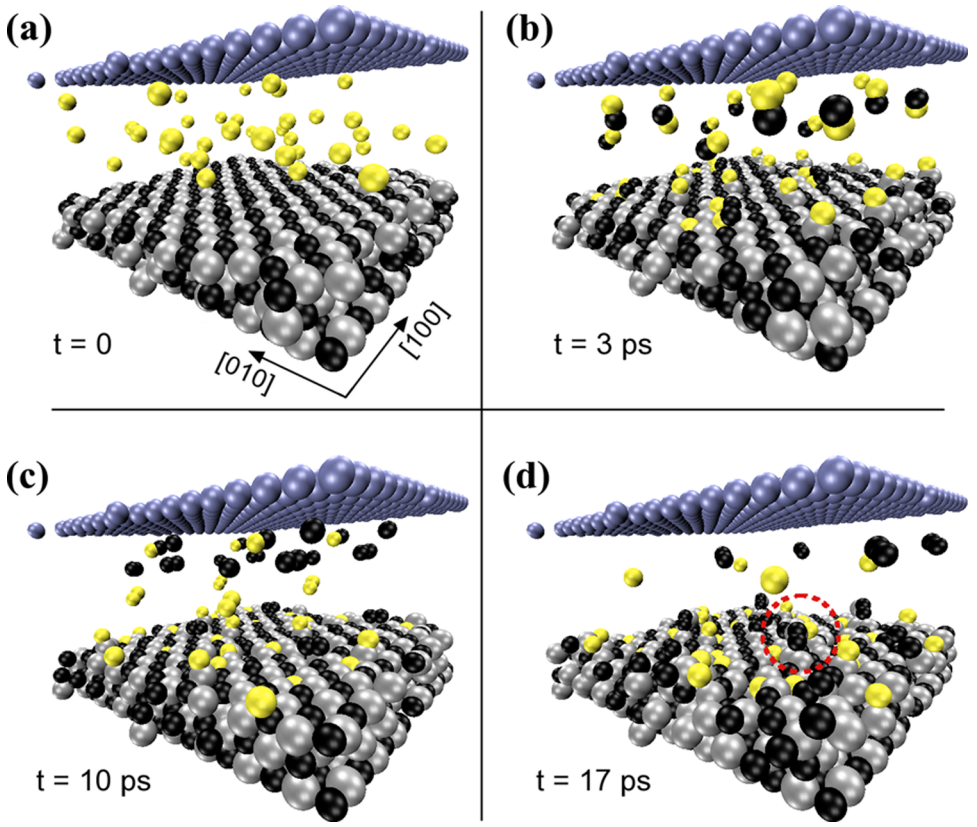

Figure 13. Images from AIMD movies of a pristine VN(001) surface exposed to N gas atoms at 1900 K. Color legend: yellow = N_{gas}, black = N_{surf}, silver = V_{surf}, blue = He barrier atoms. Each panel shows four simulation-cell replicas. The dashed red circle in panel d indicates the formation of an epitaxial V_2N_3 island. See section 3.5 and Figure 14 for further explanation.

VN(001) with approximately equal probability at atop-V and TFS positions.

Calculated average N_{ad}/N_{surf} desorption rates from VN(001), $1.0(\times 3.0^{\pm 1}) \times 10^{12}$ s^{-1} (note desorbed N_{ad}/N_{surf} molecules in Figure 13b), correspond to N adatom lifetimes of approximately 0.5 ps. Although N_{ad} surface coverages in these experiments range up to 0.2 ML, N_{ad}/N_{ad} recombination is never observed. Even when three N adatoms are located at adjacent TSF positions and/or atop-V sites, the most probable reaction pathway is N_{ad}/N_{surf} pair formation followed by exchange reactions and desorption. This suggests that N_{ad}/N_{ad} long-range interactions on VN(001) are strongly repulsive, similar to the case for N_{ad}/TiN(001).[62]

In addition to establishing that N_{ad}/N_{surf} desorption is much more likely than N_{ad}/N_{ad} recombinative desorption on VN(001), AIMD movies show that N_2 desorption can also be initiated by gas/surface collisions. The vibrational amplitude of N_2 gas molecules is perturbed and enhanced by the presence of N gas atoms. Occasionally, this leads to N−N bond breakage,[123] which produces energetic (approximately 10 eV) N_{gas} atoms. If an energetic N_{gas} species is incident at a N adatom or a N surface atom, it forms, with ∼100% probability, N_2 molecules which immediately desorb.

The creation of surface anion vacancies due to N_{ad}/N_{surf}, N_{gas}/N_{surf}, and N_{gas}/N_{ad} desorption leads to an average steady-state VN(001) surface stoichiometry of $VN_{0.96}$. In most cases, N surface vacancies are promptly filled by itinerant N adatoms or by impinging N_{gas} atoms (note, for example, the N_{gas} atoms (shown in yellow) occupying anion positions in the VN(001) surface in Figure 13c). During the N_{gas}/VN(001) simulation, we also detect the dissociation of N_2 gas molecules which happen to collide proximate to N_{vac} surface sites. As described in section 3.4, one N atom fills the vacancy while the other remains on the surface as a free N adatom.

On one occasion out of 10−15 events, the recoil of an energetic N_{gas} atom from a V_{surf} atom, Figure 13d, lifts the latter to form a VN admolecule. The presence of the VN admolecule promotes cluster growth. A nearby N_{ad} species pulls up a V_{surf} atom to form a second VN admolecule which bonds to the adjacent initial VN, thus producing an L-shape V_2N_2 cluster with all atoms in epitaxial positions. Next, an incident N_{gas} atom bonds to the V_2N_2 cluster to form a V_2N_3 epitaxial island (indicated by the dashed red circle in Figure 13d). Figure 14, a plan view image of the final simulation frame, summarizes the effects of N gas atoms on VN(001) surface morphology. The epitaxial V_2N_3 island forms together with four surface vacancies: a next-nearest neighbor cation surface vacancy pair in which one of the V vacancies is adjacent to a N_{vac} and an additional, isolated, N_{vac}.

Experimental results for epitaxial growth of $TiN_x(001)$[33,88] as well as $TaN_x(001)$[34,124] and HfN_x[95] indicate that plasma activation producing gas-phase atomic N is essential for forming stoichiometric layers. Our simulation results are consistent with the experimental reports and show that N_2 is much less reactive than atomic N since the molecular species require interaction with surface anion vacancies (see section 3.4) to promote dissociative chemisorption.

3.6. Implications for TiN(001) vs. VN(001) Catalytic Properties. In addition to elucidating the effects of nitrogen precursor fluxes and temperatures for controlling the

DOI: 10.1021/acs.jpcc.6b02652
J. Phys. Chem. C 2016, 120, 12503−12516

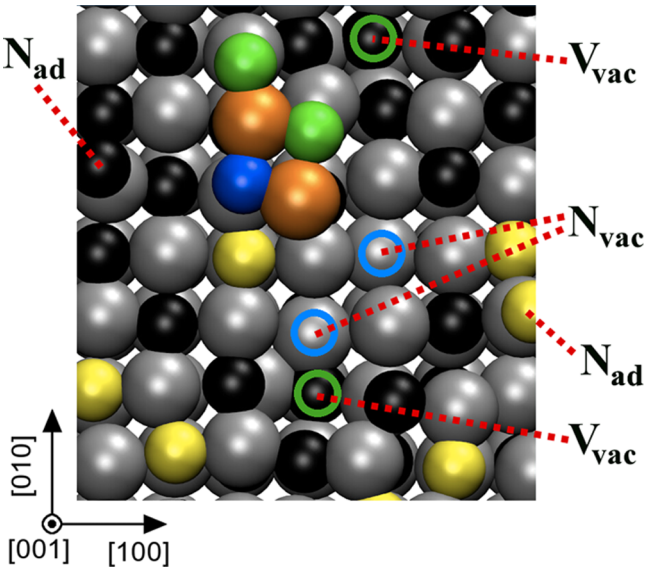

Figure 14. Images from an AIMD movie of VN(001) exposed to N gas atoms. Color legend: yellow = N_{gas}, black = N_{surf}, silver = V_{surf}, orange = V island atom, green = N island atom (originally N_{gas}), blue = N island atom (originally N_{surf}), open blue circle = N_{vac}, and open green circle = V_{vac}. N_{vac} and V_{vac} indicate anion and cation surface vacancies, respectively. N_{ad} = nitrogen adatoms. See text, section 3.5, for further discussion.

stoichiometry of TM nitride (001) layers, the results described in the previous sections demonstrate the ability of surface anion vacancies to catalyze N_2 dissociation on VN(001) as well as on TiN(001) surfaces[62] and suggest a route to tune the catalytic reactivity of these surfaces. An example is the formation of ammonia at ambient conditions.[51,52]

It has recently been suggested that free N adatoms on NaCl-structure TM nitride (001) surfaces[51] promote NH_4^+ formation upon hydrogenation. However, this reaction requires constant availability and reactivity of N adatoms. On TiN(001), N adatoms immediately form strong bonds with N surface atoms, as shown by AIMD simulations[62] and by the considerably larger N adatom adsorption energies in TFS than in FFH or atop-Ti_{surf} positions.[117] Strong N_{ad}/N_{surf} bonds do not favor N_{ad} hydrogenation and release of ammonia. N_{ad} species in TFS positions on VN(001) are also highly stable due to the strong N_{ad}/N_{surf} bond; however, the formation of N_{ad}/N_{surf} pairs on VN(001) is kinetically hindered, as demonstrated by adatom surface migration rates being much higher than N_{ad}/N_{surf} desorption rates for T below 1000 K (Figure 9).

The relatively high stability of N adatoms on epitaxial atop-V sites on VN(001), explained by means of temperature-dependent ab initio electronic structures demonstrating that an additional valence electron in VN vs. TiN strengthens both σ $N_{ad}(p_z)-TM_{surf}(d_z^2)$ and π $N_{ad}(p_x + p_y)-TM_{surf}(d_{xz} + d_{yz})$ bonding (section 3.2), yields N_{ad} surface migration rates which are considerably higher than N_{ad}/N_{surf} desorption rates at room temperature (Figure 9). Thus, itinerant N adatoms have a high probability to bond with hydrogen atoms, favoring ammonia formation and desorption at 300 K.

In summary, the reactivity of N adatoms on TM nitride (001) surfaces increases with surface ECAS electron concentrations due to nitrogen species evolving from being essentially chemically inert N_2 (N_{ad}/N_{surf}) molecules (ECAS $\leq$ 14) to chemically reactive N adatoms (ECAS > 14).

4. CONCLUSIONS

Density-functional AIMD simulations show that N adatoms on VN(001), at temperatures ranging from 1600 to 2300 K, prefer epitaxial atop-V positions and diffuse among them by transiting through 4-fold hollow sites. From FFH positions, N_{ad} species can also reach stable 3-fold sites, close to a N surface atom and bounded by two V atoms. In this position, N adatoms form strongly-bonded N_{ad}/N_{surf} pairs which, after several N_{ad}/N_{surf} exchange reactions, desorb leaving an anion surface vacancy. N surface vacancies rapidly migrate in plane via ⟨110⟩ jumps and act as efficient catalysts for the dissociative chemisorption of incident N_2 molecules. AIMD simulations of VN(001) exposed to gas-phase N atoms reveal that even at high N_{ad} surface coverages (e.g., two or even three N adatoms located on adjacent TFS or atop-V positions), N_{ad}/N_{ad} recombination and desorption is never observed. Instead, N_2 loss occurs by N_{ad}/N_{surf} desorption and by energetic N_{gas} atoms colliding with N_{ad} or N_{surf} species to form molecules which immediately desorb. The formation of metastable VN admolecules, due to an itinerant N_{ad} pulling a V substrate atom onto the surface, can lead to growth of larger clusters via capture of incident N gas atoms.

Comparison with our previous results for N_{ad} migration on and N_2 desorption from TiN(001) show that on both VN(001) and TiN(001) surfaces, N_2 molecule formation and desorption is primarily initiated by N adatoms removing a N surface atom and desorbing as N_{ad}/N_{surf} rather than by N_{ad}/N_{ad} recombinative desorption. However, on VN(001), N_{ad} species reside primarily on surface atop-V epitaxial sites rather than at TFS positions, the preferential N_{ad}/TiN(001) adsorption sites, due to an additional valence electron per formula unit for VN(001) vs. TiN(001) which strengthens N_{ad}/TM_{surf} bonding. This yields, for temperatures less than 1000 K, significantly higher N_{ad} average migration distances on VN(001) compared to TiN(001) prior to N_{ad}/N_{surf} desorption.

The present findings explain why plasma activation during reactive sputter deposition plays such a crucial role for forming stoichiometric TM nitride (001) layers: gas-phase N_2 is much less reactive than atomic N since the molecular species require interaction with surface anion vacancies to initiate dissociation. Our results also provide direct insights for controlling the catalytic reactivity of TM nitride (001) surfaces via electron-concentration tuning.

AUTHOR INFORMATION

Corresponding Author

*Phone: 0046 13282623. Fax: 0046 13137568. E-mail: davsan@ifm.liu.se.

Notes

The authors declare no competing financial interest.

ACKNOWLEDGMENTS

This research was carried out using resources provided by the Swedish National Infrastructure for Computing (SNIC), on the Gamma, Triolith, Matter, and Kappa Clusters located at the National Supercomputer Centre (NSC) in Linköping, and on the Beskow cluster located at the Center for High Performance Computing (PDC) in Stockholm, Sweden. W. Olovsson and P. Münger at NSC and H. Leskelä and J. Vincent at PDC are acknowledged for assistance with technical aspects. We gratefully acknowledge financial support from the Knut and Alice Wallenberg Foundation (Isotope Project No. 2011.0094),

DOI: 10.1021/acs.jpcc.6b02652
J. Phys. Chem. C 2016, 120, 12503−12516

the Swedish Research Council (VR) Linköping Linnaeus Initiative LiLi-NFM (Grant No. 2008-6572) and Project Grant Nos. 2014-5790 and 2013-4018), and the Swedish Government Strategic Research Area Grant in Materials Science on Advanced Functional Materials (Grant No. MatLiU 2009-00971 through Sweden's innovation agency VINNOVA).

REFERENCES

(1) Mayrhofer, P. H.; Mitterer, C.; Hultman, L.; Clemens, H. Microstructural design of hard coatings. *Prog. Mater. Sci.* **2006**, *51*, 1032−1114.
(2) Abadias, G.; Koutsokeras, L. E.; Dub, S. N.; Tolmachova, G. N.; Debelle, A.; Sauvage, T.; Villechaise, P. Reactive magnetron cosputtering of hard and conductive ternary nitride thin films: Ti-Zr-N and Ti-Ta-N. *J. Vac. Sci. Technol., A* **2010**, *28*, 541−551.
(3) Yu, S.; Zeng, Q.; Oganov, A. R.; Frapper, G.; Zhang, L. Phase stability, chemical bonding and mechanical properties of titanium nitrides: a first-principles study. *Phys. Chem. Chem. Phys.* **2015**, *17*, 11763−11769.
(4) Kindlund, H.; Sangiovanni, D. G.; Martinez-de-Olcoz, L.; Lu, J.; Jensen, J.; Birch, J.; Petrov, I.; Greene, J. E.; Chirita, V.; Hultman, L. Toughness enhancement in hard ceramic thin films by alloy design. *APL Mater.* **2013**, *1*, 042104.
(5) Kindlund, H.; Sangiovanni, D. G.; Lu, J.; Jensen, J.; Chirita, V.; Petrov, I.; Greene, J. E.; Hultman, L. Effect of WN content on toughness enhancement in $V_{1-x}W_xN$/MgO(001) thin films. *J. Vac. Sci. Technol., A* **2014**, *32*, 030603.
(6) Ding, X. Z.; Tan, A. L. K.; Zeng, X. T.; Wang, C.; Yue, T.; Sun, C. Q. Corrosion resistance of CrAlN and TiAlN coatings deposited by lateral rotating cathode arc. *Thin Solid Films* **2008**, *516*, 5716−5720.
(7) Kayali, Y. The corrosion and wear behavior of TiN and TiAlN coated AISI 316 L stainless steel. *Prot. Met. Phys. Chem. Surf.* **2014**, *50*, 412−419.
(8) Gall, D.; Petrov, I.; Greene, J. E. Epitaxial $Sc_{1-x}Ti_xN(001)$: Optical and electronic transport properties. *J. Appl. Phys.* **2001**, *89*, 401−409.
(9) Gall, D.; Stoehr, M.; Greene, J. E. Vibrational modes in epitaxial $Ti_{1-x}Sc_xN(001)$ layers: An *ab initio* calculation and Raman spectroscopy study. *Phys. Rev. B: Condens. Matter Mater. Phys.* **2001**, *64*, 174302.
(10) Gall, D.; Shin, C. S.; Haasch, R. T.; Petrov, I.; Greene, J. E. Band gap in epitaxial NaCl-structure CrN(001) layers. *J. Appl. Phys.* **2002**, *91*, 5882−5886.
(11) Uglov, V. V.; Anishchik, V. M.; Zlotski, S. V.; Abadias, G.; Dub, S. N. Structural and mechanical stability upon annealing of arc-deposited Ti-Zr-N coatings. *Surf. Coat. Technol.* **2008**, *202*, 2394−2398.
(12) Mei, A. B.; Rockett, A.; Hultman, L.; Petrov, I.; Greene, J. E. Electron/phonon coupling in group-IV transition-metal and rare-earth nitrides. *J. Appl. Phys.* **2013**, *114*, 193708.
(13) Ning, L.; Veldhuis, S. C.; Yamamoto, K. Investigation of wear behavior and chip formation for cutting tools with nano-multilayered TiAlCrN/NbN PVD coating. *International Journal of Machine Tools & Manufacture* **2008**, *48*, 656−665.
(14) Wolfe, D. E.; Gabriel, B. M.; Reedy, M. W. Nanolayer (Ti,Cr)N coatings for hard particle erosion resistance. *Surf. Coat. Technol.* **2011**, *205*, 4569−4576.
(15) Ruan, J. L.; Lii, D. F.; Chen, J. S.; Huang, J. L. Investigation of substrate bias effects on the reactively sputtered ZrN diffusion barrier films. *Ceram. Int.* **2009**, *35*, 1999−2005.
(16) Koutsokeras, L. E.; Abadias, G.; Lekka, C. E.; Matenoglou, G. M.; Anagnostopoulos, D. F.; Evangelakis, G. A.; Patsalas, P. Conducting transition metal nitride thin films with tailored cell sizes: The case of δ-$Ti_xTa_{1-x}N$. *Appl. Phys. Lett.* **2008**, *93*, 011904.
(17) Kuo, Y. L.; Lee, H. H.; Lee, C.; Lin, J. C.; Shue, S. L.; Liang, M. S.; Daniels, B. J. Diffusion of copper in titanium zirconium nitride thin films. *Electrochem. Solid-State Lett.* **2004**, *7*, C35−C37.
(18) Knoops, H. C. M.; Baggetto, L.; Langereis, E.; van de Sanden, M. C. M.; Klootwijk, J. H.; Roozeboom, F.; Niessen, R. A. H.; Notten, P. H. L.; Kessels, W. M. M. Deposition of TiN and TaN by remote plasma ALD for Cu and Li diffusion barrier applications. *J. Electrochem. Soc.* **2008**, *155*, G287−G294.
(19) Eklund, P.; Kerdsongpanya, S.; Alling, B. Transition-metal-nitride-based thin films as novel energy harvesting materials. *J. Mater. Chem. C* **2016**, *4*, 3905.
(20) Zhang, L.; Holt, C. M. B.; Luber, E. J.; Olsen, B. C.; Wang, H.; Danaie, M.; Cui, X.; Tan, X.; Lui, V. W.; Kalisvaart, W. P.; Mitlin, D. High rate electrochemical capacitors from three-dimensional arrays of vanadium nitride functionalized carbon nanotubes. *J. Phys. Chem. C* **2011**, *115*, 24381−24393.
(21) Patsalas, P.; Kalfagiannis, N.; Kassavetis, S. Optical properties and plasmonic performance of titanium nitride. *Materials* **2015**, *8*, 3128−3154.
(22) Naik, G. V.; Kim, J.; Boltasseva, A. Oxides and nitrides as alternative plasmonic materials in the optical range. *Opt. Mater. Express* **2011**, *1*, 1090−1099.
(23) Guler, U.; Boltasseva, A.; Shalaev, V. M. Refractory plasmonics. *Science* **2014**, *344*, 263−264.
(24) Ramanathan, S.; Oyama, S. T. New catalysts for hydroprocessing - Transition-metal carbides and nitrides. *J. Phys. Chem.* **1995**, *99*, 16365−16372.
(25) Wu, M.; Guo, H.; Lin, Y.-n.; Wu, K.; Ma, T.; Hagfeldt, A. Synthesis of highly effective vanadium nitride (VN) peas as a counter electrode catalyst in dye-sensitized solar cells. *J. Phys. Chem. C* **2014**, *118*, 12625−12631.
(26) Chen, J. G. G. Carbide and nitride overlayers on early transition metal surfaces: Preparation, characterization, and reactivities. *Chem. Rev.* **1996**, *96*, 1477−1498.
(27) Oyama, S. T. *The chemistry of transition metal carbides and nitrides*; Blackie Academic & Professional: Glasgow, 1996.
(28) Gupta, A.; Wang, H.; Kvit, A.; Duscher, G.; Narayan, J. Effect of microstructure on diffusion of copper in TiN films. *J. Appl. Phys.* **2003**, *93*, 5210−5214.
(29) Chun, J. S.; Petrov, I.; Greene, J. E. Dense fully 111-textured TiN diffusion barriers: Enhanced lifetime through microstructure control during layer growth. *J. Appl. Phys.* **1999**, *86*, 3633−3641.
(30) Petrov, I.; Barna, P. B.; Hultman, L.; Greene, J. E. Microstructural evolution during film growth. *J. Vac. Sci. Technol., A* **2003**, *21*, S117−S128.
(31) Helmersson, U.; Sundgren, J. E.; Greene, J. E. Microstructure evolution in TiN films reactively sputter deposited on multiphase substrates. *J. Vac. Sci. Technol., A* **1986**, *4*, 500−503.
(32) Baumann, F. H.; Chopp, D. L.; de la Rubia, T. D.; Gilmer, G. H.; Greene, J. E.; Huang, H.; Kodambaka, S.; O'Sullivan, P.; Petrov, I. Multiscale modeling of thin-film deposition: Applications to Si device processing. *MRS Bull.* **2001**, *26*, 182−189.
(33) Lee, T.; Ohmori, K.; Shin, C. S.; Cahill, D. G.; Petrov, I.; Greene, J. E. Elastic constants of single-crystal $TiN_x(001)$ ($0.67 \leq x \leq 1.0$) determined as a function of x by picosecond ultrasonic measurements. *Phys. Rev. B: Condens. Matter Mater. Phys.* **2005**, *71*, 144106.
(34) Shin, C. S.; Gall, D.; Kim, Y. W.; Desjardins, P.; Petrov, I.; Greene, J. E.; Oden, M.; Hultman, L. Epitaxial NaCl structure δ-$TaN_x(001)$: Electronic transport properties, elastic modulus, and hardness versus N/Ta ratio. *J. Appl. Phys.* **2001**, *90*, 2879−2885.
(35) Shin, C. S.; Gall, D.; Hellgren, N.; Patscheider, J.; Petrov, I.; Greene, J. E. Vacancy hardening in single-crystal $TiN_x(001)$ layers. Greene. *J. Appl. Phys.* **2003**, *93*, 6025−6028.
(36) Sundgren, J. E. Structure and properties of TiN coatings. *Thin Solid Films* **1985**, *128*, 21−44.
(37) Greene, J. E.; Sundgren, J. E.; Hultman, L.; Petrov, I.; Bergstrom, D. B. Development of preferred orientation in polycrystalline TiN layers grown by ultrahigh-vacuum reactive magnetron sputtering. *Appl. Phys. Lett.* **1995**, *67*, 2928−2930.
(38) Bareno, J.; Kodambaka, S.; Khare, S. V.; Swiech, W.; Petrova, V.; Petrov, I.; Greene, J. E. *TiN surface dynamics: Role of surface and bulk mass transport processes*; Advanced Summer School in Physics: Mexico City, Mexico, 2006; pp 205−224.

DOI: 10.1021/acs.jpcc.6b02652
J. Phys. Chem. C 2016, 120, 12503−12516

(39) Kodambaka, S.; Petrova, V.; Vailionis, A.; Desjardins, P.; Cahill, D. G.; Petrov, I.; Greene, J. E. In-situ high-temperature scanning-tunnelling-microscopy studies of two-dimensional island-decay kinetics on atomically smooth TiN(001). *Surf. Rev. Lett.* **2000**, *7*, 589−593.
(40) Kodambaka, S.; Khare, S. V.; Petrova, V.; Vailionis, A.; Petrov, I.; Greene, J. E. Absolute orientation-dependent TiN(001) step energies from two-dimensional equilibrium island shape and coarsening measurements on epitaxial TiN(001) layers. *Surf. Sci.* **2002**, *513*, 468−474.
(41) Kodambaka, S.; Chopp, D. L.; Petrov, I.; Greene, J. E. Coalescence kinetics of two-dimensional TiN islands on atomically smooth TiN(001) and TiN(111) terraces. *Surf. Sci.* **2003**, *540*, L611−L616.
(42) Karr, B. W.; Petrov, I.; Cahill, D. G.; Greene, J. E. Morphology of epitaxial TiN(001) grown by magnetron sputtering. *Appl. Phys. Lett.* **1997**, *70*, 1703−1705.
(43) Liu, G. H.; Chen, K. X.; Zhou, H. P.; Tian, J. J.; Pereira, C.; Ferreira, J. M. F. Fast shape evolution of TiN microcrystals in combustion synthesis. *Cryst. Growth Des.* **2006**, *6*, 2404−2411.
(44) Kaskel, S.; Schlichte, K.; Chaplais, G.; Khanna, M. Synthesis and characterisation of titanium nitride based nanoparticles. *J. Mater. Chem.* **2003**, *13*, 1496−1499.
(45) Drygas, M.; Czosnek, C.; Paine, R. T.; Janik, J. F. Two-stage aerosol synthesis of titanium nitride TiN and titanium oxynitride TiO_xN_y nanopowders of spherical particle morphology. *Chem. Mater.* **2006**, *18*, 3122−3129.
(46) Wiklund, U.; Casas, B.; Stavlid, N. Evaporated vanadium nitride as a friction material in dry sliding against stainless steel. *Wear* **2006**, *261*, 2−8.
(47) Qiu, Y.; Zhang, S.; Li, B.; Wang, Y.; Lee, J.-W.; Li, F.; Zhao, D. Improvement of tribological performance of CrN coating via multilayering with VN. *Surf. Coat. Technol.* **2013**, *231*, 357−363.
(48) Choi, D.; Blomgren, G. E.; Kumta, P. N. Fast and reversible surface redox reaction in nanocrystalline vanadium nitride supercapacitors. *Adv. Mater.* **2006**, *18*, 1178.
(49) Zhang, K. J.; Wang, H. B.; He, X. Q.; Liu, Z. H.; Wang, L.; Gu, L.; Xu, H. X.; Han, P. X.; Dong, S. M.; Zhang, C. J.; Yao, J. H.; Cui, G. L.; Chen, L. Q. A hybrid material of vanadium nitride and nitrogen-doped graphene for lithium storage. *J. Mater. Chem.* **2011**, *21*, 11916−11922.
(50) Sun, Q.; Fu, Z. W. Vanadium nitride as a novel thin film anode material for rechargeable lithium batteries. *Electrochim. Acta* **2008**, *54*, 403−409.
(51) Abghoui, Y.; Garden, A. L.; Hlynsson, V. F.; Bjorgvinsdottir, S.; Olafsdottir, H.; Skúlason, E. Enabling electrochemical reduction of nitrogen to ammonia at ambient conditions through rational catalyst design. *Phys. Chem. Chem. Phys.* **2015**, *17*, 4909−4918.
(52) Abghoui, Y.; Garden, A. L.; Howalt, J. G.; Vegge, T.; Skúlason, E. Electroreduction of N_2 to ammonia at ambient conditions on mononitrides of Zr, Nb, Cr, and V: A DFT Guide for experiments. *ACS Catal.* **2016**, *6*, 635−646.
(53) Watanabe, F.; Kodambaka, S.; Swiech, W.; Greene, J. E.; Cahill, D. G. LEEM study of island decay on Si(110). *Surf. Sci.* **2004**, *572*, 425−432.
(54) Tsetseris, L.; Logothetidis, S.; Pantelides, S. T. Migration of species in a prototype diffusion barrier: Cu, O, and H in TiN. *Appl. Phys. Lett.* **2009**, *94*, 161903.
(55) Vojvodic, A.; Ruberto, C.; Lundqvist, B. I. Trends in atomic adsorption on titanium carbide and nitride. *Surf. Sci.* **2006**, *600*, 3619−3623.
(56) Ren, Y.; Liu, X. J.; Tan, X.; Westkamper, E. Adsorption and pathways of single atomistic processes on TiN (111) surfaces: A first principle study. *Comput. Mater. Sci.* **2013**, *77*, 102−107.
(57) Tholander, C.; Alling, B.; Tasnádi, F.; Greene, J. E.; Hultman, L. Effect of Al substitution on Ti, Al, and N adatom dynamics on TiN(001), (011), and (111) surfaces. *Surf. Sci.* **2014**, *630*, 28−40.
(58) Wert, C.; Zener, C. Interstitial atomic diffusion coefficients. *Phys. Rev.* **1949**, *76*, 1169.
(59) Vineyard, G. H. Frequency factors and isotope effects in solid state rate processes. *J. Phys. Chem. Solids* **1957**, *3*, 121.
(60) Mei, A. B.; Hellman, O.; Wireklint, N.; Schlepütz, C. M.; Sangiovanni, D. G.; Alling, B.; Rockett, A.; Hultman, L.; Petrov, I.; Greene, J. E. Dynamic and structural stability of cubic vanadium nitride. *Phys. Rev. B: Condens. Matter Mater. Phys.* **2015**, *91*, 054101.
(61) Isaev, E. I.; Simak, S. I.; Abrikosov, I. A.; Ahuja, R.; Vekilov, Y. K.; Katsnelson, M. I.; Lichtenstein, A. I.; Johansson, B. Phonon related properties of transition metals, their carbides, and nitrides: A first-principles study. *J. Appl. Phys.* **2007**, *101*, 123519.
(62) Sangiovanni, D. G.; Edström, D.; Hultman, L.; Petrov, I.; Greene, J. E.; Chirita, V. *Ab initio* and classical molecular dynamics simulations of N_2 desorption from TiN(001) surfaces. *Surf. Sci.* **2014**, *624*, 25−31.
(63) Sangiovanni, D. G.; Alling, B.; Steneteg, P.; Hultman, L.; Abrikosov, I. A. Nitrogen vacancy, self-interstitial diffusion, and Frenkel-pair formation/dissociation in B1 TiN studied by *ab initio* and classical molecular dynamics with optimized potentials. *Phys. Rev. B: Condens. Matter Mater. Phys.* **2015**, *91*, 054301.
(64) Music, D.; Schneider, J. M. *Ab initio* study of $Ti_{0.5}Al_{0.5}N(001)$-residual and environmental gas interactions. *New J. Phys.* **2013**, *15*, 073004.
(65) Piscanec, S.; Ciacchi, L. C.; Vesselli, E.; Comelli, G.; Sbaizero, O.; Meriani, S.; De Vita, A. Bioactivity of TiN-coated titanium implants. *Acta Mater.* **2004**, *52*, 1237−1245.
(66) Edström, D.; Sangiovanni, D. G.; Hultman, L.; Chirita, V.; Petrov, I.; Greene, J. E. Ti and N adatom descent pathways to the terrace from atop two-dimensional TiN/TiN(001) islands. *Thin Solid Films* **2014**, *558*, 37−46.
(67) Sangiovanni, D. G.; Edström, D.; Hultman, L.; Chirita, V.; Petrov, I.; Greene, J. E. Dynamics of Ti, N, and TiN_x (x = 1−3) admolecule transport on TiN(001) surfaces. *Phys. Rev. B: Condens. Matter Mater. Phys.* **2012**, *86*, 155443.
(68) Sangiovanni, D. G.; Edström, D.; Hultman, L.; Petrov, I.; Greene, J. E.; Chirita, V. Ti adatom diffusion on TiN(001): *Ab initio* and classical molecular dynamics simulations. *Surf. Sci.* **2014**, *627*, 34−41.
(69) Edström, D.; Sangiovanni, D. G.; Hultman, L.; Petrov, I.; Greene, J. E.; Chirita, V. The dynamics of TiN_x (x = 1−3) admolecule interlayer and intralayer transport on TiN/TiN(001) islands. *Thin Solid Films* **2015**, *589*, 133.
(70) Sangiovanni, D. G.; Tasnadi, F.; Hultman, L.; Petrov, I.; Greene, J. E.; Chirita, V. N and Ti adatom dynamics on stoichiometric polar TiN(111) surfaces. *Surf. Sci.* **2016**, *649*, 72−79.
(71) Rodriguez, J. A.; Liu, P.; Dvorak, J.; Jirsak, T.; Gomes, J.; Takahashi, Y.; Nakamura, K. The interaction of oxygen with TiC(001): Photoemission and first-principles studies. *J. Chem. Phys.* **2004**, *121*, 465−474.
(72) Rodriguez, J. A.; Liu, P.; Gomes, J.; Nakamura, K.; Vines, F.; Sousa, C.; Illas, F. Interaction of oxygen with ZrC(001) and VC(001): Photoemission and first-principles studies. *Phys. Rev. B: Condens. Matter Mater. Phys.* **2005**, *72*, 075427.
(73) Vines, F.; Sousa, C.; Illas, F.; Liu, P.; Rodriguez, J. A. Density functional study of the adsorption of atomic oxygen on the (001) surface of early transition-metal carbides. *J. Phys. Chem. C* **2007**, *111*, 1307−1314.
(74) Kitaoka, H.; Ozawa, K.; Edamoto, K.; Otani, S. Electronic structure of the Zr suboxide layer formed on a ZrC(100) surface. *Surf. Sci.* **2002**, *511*, 359−365.
(75) Shirotori, Y.; Sawada, K.; Ozawa, K.; Edamoto, K.; Otani, S. Electronic structure of the Ti suboxide layer formed on a TiC(100) surface: Angle-resolved photoemission study. *Surf. Sci.* **2005**, *584*, 237−244.
(76) Souda, R.; Aizawa, T.; Otani, S.; Ishizawa, Y.; Oshima, C. Oxygen chemisorption on transition metal carbide (100) surfaces studied by X-ray photoelectron spectroscopy and low-energy He^+ scattering. *Surf. Sci.* **1991**, *256*, 19−26.

DOI: 10.1021/acs.jpcc.6b02652
J. Phys. Chem. C 2016, 120, 12503−12516

(77) Graciani, J.; Fernández Sanz, J.; Asaki, T.; Nakamura, K.; Rodriguez, J. A. Interaction of oxygen with TiN(001): N ←→ O exchange and oxidation process. *J. Chem. Phys.* **2007**, *126*, 244713.
(78) Graciani, J.; Fernández Sanz, J.; Marquez, A. M. A Density functional study of initial steps in the oxidation of early transition metal nitrides, MN (M = Sc, Ti, and V). *J. Phys. Chem. C* **2009**, *113*, 930−938.
(79) Hong, M.; Lee, D.-H.; Phillpot, S. R.; Sinnott, S. B. A mechanism for TiO_2 formation on stepped TiN(001) from first-principles calculations. *J. Phys. Chem. C* **2014**, *118*, 384−388.
(80) Frantz, P.; Didziulis, S. V. Detailed spectroscopic studies of oxygen on metal carbide surfaces. *Surf. Sci.* **1998**, *412-413*, 384−396.
(81) Kunze, C.; Music, D.; Baben, M. T.; Schneider, J. M.; Grundmeier, G. Temporal evolution of oxygen chemisorption on TiAlN. *Appl. Surf. Sci.* **2014**, *290*, 504−508.
(82) Tsong, T. T. Field-ion microscope observations of indirect interaction between adatoms on metal surfaces. *Phys. Rev. Lett.* **1973**, *31*, 1207.
(83) Watanabe, F.; Ehrlich, G. Direct mapping of adatom-adatom interactions. *Phys. Rev. Lett.* **1989**, *62*, 1146−1149.
(84) Lau, K. H.; Kohn, W. Elastic interaction of two atoms adsorbed on a solid surface. *Surf. Sci.* **1977**, *65*, 607−618.
(85) Lau, K. H.; Kohn, W. Indirect long-range oscillatory interaction between adsorbed atoms. *Surf. Sci.* **1978**, *75*, 69−85.
(86) Lee, J. S.; Zhang, Z.; Deng, X. Y.; Sorescu, D. C.; Matranga, C.; Yates, J. T. Interaction of CO with oxygen adatoms on TiO_2(110). *J. Phys. Chem. C* **2011**, *115*, 4163−4167.
(87) Zorn, D. D.; Albao, M. A.; Evans, J. W.; Gordon, M. S. Binding and diffusion of Al adatoms and dimers on the Si(100)-2 × 1 reconstructed surface: A hybrid QM/MM embedded cluster study. *J. Phys. Chem. C* **2009**, *113*, 7277−7289.
(88) Shin, C. S.; Rudenja, S.; Gall, D.; Hellgren, N.; Lee, T. Y.; Petrov, I.; Greene, J. E. Growth, surface morphology, and electrical resistivity of fully strained substoichiometric epitaxial TiNx ($0.67 \leq x < 1.0$) layers on MgO(001). *J. Appl. Phys.* **2004**, *95*, 356−362.
(89) Chhowalla, M.; Unalan, H. E. Thin films of hard cubic Zr_3N_4 stabilized by stress. *Nat. Mater.* **2005**, *4*, 317−322.
(90) Xu, M.; Wang, S.; Yin, G.; Li, J.; Zheng, Y.; Chen, L.; Jia, Y. Optical properties of cubic Ti_3N_4, Zr_3N_4, and Hf_3N_4. *Appl. Phys. Lett.* **2006**, *89*, 151908.
(91) Porte, L.; Roux, L.; Hanus, J. Vacancy effects in the X-ray photoelectron spectra of TiN_x. *Phys. Rev. B: Condens. Matter Mater. Phys.* **1983**, *28*, 3214.
(92) Kang, J. H.; Kim, K. J. Structural, optical, and electronic properties of cubic TiN_x compounds. *J. Appl. Phys.* **1999**, *86*, 346−350.
(93) Gu, Z.; Hu, C.; Huang, H.; Zhang, S.; Fan, X.; Wang, X.; Zheng, W. Identification and thermodynamic mechanism of the phase transition in hafnium nitride films. *Acta Mater.* **2015**, *90*, 59.
(94) Seo, H. S.; Lee, T. Y.; Wen, J. G.; Petrov, I.; Greene, J. E.; Gall, D. Growth and physical properties of epitaxial HfN layers on MgO(001). *J. Appl. Phys.* **2004**, *96*, 878−884.
(95) Seo, H. S.; Lee, T. Y.; Petrov, I.; Greene, J. E.; Gall, D. Epitaxial and polycrystalline HfN_x ($0.8 \leq x \leq 1.5$) layers on MgO(001): Film growth and physical properties. *J. Appl. Phys.* **2005**, *97*, 083521.
(96) Shin, C. S.; Kim, Y. W.; Hellgren, N.; Gall, D.; Petrov, I.; Greene, J. E. Epitaxial growth of metastable δ-TaN layers on MgO(001) using low-energy, high-flux ion irradiation during ultrahigh vacuum reactive magnetron sputtering. *J. Vac. Sci. Technol., A* **2002**, *20*, 2007−2017.
(97) Michalsky, R.; Pfromm, P. H. An ionicity rationale to design solid phase metal nitride reactants for solar ammonia production. *J. Phys. Chem. C* **2012**, *116*, 23243−23251.
(98) Rodriguez, P.; Brito, J.; Albornoz, A.; Labadi, M.; Pfaff, C.; Marrero, S.; Moronta, D.; Betancourt, P. Comparison of vanadium carbide and nitride catalysts for hydrotreating. *Catal. Commun.* **2004**, *5*, 79−82.
(99) Kindlund, H.; Sangiovanni, D. G.; Lu, J.; Jensen, J.; Chirita, V.; Birch, J.; Petrov, I.; Greene, J. E.; Hultman, L. Vacancy-induced toughening in hard single-crystal $V_{0.5}Mo_{0.5}N_x$/MgO(001) thin films. *Acta Mater.* **2014**, *77*, 394.
(100) Kresse, G.; Hafner, J. *Ab initio* molecular dynamics for liquid metals. *Phys. Rev. B: Condens. Matter Mater. Phys.* **1993**, *47*, 558.
(101) Perdew, J. P.; Burke, K.; Wang, Y. Generalized gradient approximation for the exchange-correlation hole of a many-electron system. *Phys. Rev. B: Condens. Matter Mater. Phys.* **1996**, *54*, 16533−16539.
(102) Blöchl, P. E. Projector augmented-wave method. *Phys. Rev. B: Condens. Matter Mater. Phys.* **1994**, *50*, 17953−17979.
(103) Humphrey, W.; Dalke, A.; Schulten, K. VMD: Visual molecular dynamics. *J. Mol. Graphics* **1996**, *14*, 33−38.
(104) Lengauer, W.; Ettmayer, P. Lattice parameters and thermal expansion of δ-VN_{1-x} from 298 to 1000 K. *Monatsh. Chem.* **1986**, *117*, 713−719.
(105) Brune, H.; Bromann, K.; Roder, H.; Kern, K.; Jacobsen, J.; Stoltze, P.; Jacobsen, K.; Norskov, J. Effect of strain on surface-diffusion and nucleation. *Phys. Rev. B: Condens. Matter Mater. Phys.* **1995**, *52*, R14380−R14383.
(106) Carlson, O. N.; Smith, J. F.; Nafziger, R. H. The vanadium-nitrogen system - A review. *Metall. Mater. Trans. A* **1986**, *17*, 1647−1656.
(107) Wang, W. E.; Kim, Y. S.; Hong, H. S. Characterization of the vanadium-nitrogen system with nitrogen pressure isobars. *J. Alloys Compd.* **2000**, *308*, 147−152.
(108) Pierson, H. O. *Handbook of refractory carbides & nitrides: Properties, characteristics, processing and apps*; Elsevier: New York, 1996.
(109) Mei, A. B.; Wilson, R. B.; Li, D.; Cahill, D. G.; Rockett, A.; Birch, J.; Hultman, L.; Greene, J. E.; Petrov, I. Elastic constants, Poisson ratios, and the elastic anisotropy of VN(001), (011), and (111) epitaxial layers grown by reactive magnetron sputter deposition. *J. Appl. Phys.* **2014**, *115*, 214908.
(110) Teichmann, C.; Lengauer, W.; Ettmayer, P.; Bauer, J.; Bohn, M. Reaction diffusion and phase equilibria in the V-N system. *Metall. Mater. Trans. A* **1997**, *28*, 837−842.
(111) Christensen, A. N.; Roehammer, P. Crystal growth of δ-VN by floating zone and zone annealing techniques. *J. Cryst. Growth* **1977**, *38*, 281−283.
(112) Petrov, I.; Adibi, F.; Greene, J. E.; Sproul, W. D.; Munz, W. D. Use of an externally applied axial magnetic field to control ion/neutral flux ratios incident at the substrate during magnetron sputter deposition. *J. Vac. Sci. Technol., A* **1992**, *10*, 3283−3287.
(113) Neugebauer, J.; Scheffler, M. Adsorbate-substrate and adsorbate-adsorbate interactions of Na and K adlayers on Al(111). *Phys. Rev. B: Condens. Matter Mater. Phys.* **1992**, *46*, 16067−16080.
(114) Mulliken, R. S. Electronic population analysis on LCAO−MO molecular wave functions. I. *J. Chem. Phys.* **1955**, *23*, 1833−1840.
(115) Mulliken, R. S. Electronic population analysis on LCAO−MO molecular wave functions. II. Overlap populations, bond orders, and covalent bond energies. *J. Chem. Phys.* **1955**, *23*, 1841−1846.
(116) The cohesive energy and melting point for pure Ti and V are 4.85 eV/atom and 1941 K vs. 5.31 eV/atom and 2183 K. Kittel, C. *Introduction to Solid State Physics*, 8th ed.,; John Wiley & Son: Hoboken, NJ, 2005.
(117) Gall, D.; Kodambaka, S.; Wall, M. A.; Petrov, I.; Greene, J. E. Pathways of atomistic processes on TiN(001) and (111) surfaces during film growth: an *ab initio* study. *J. Appl. Phys.* **2003**, *93*, 9086−9094.
(118) Mozafari, E.; Alling, B.; Steneteg, P.; Abrikosov, I. A. Role of N defects in paramagnetic CrN at finite temperatures from first principles. *Phys. Rev. B: Condens. Matter Mater. Phys.* **2015**, *91*, 094101.
(119) Assuming that the Arrhenius relationships continue below 1500 K, lowest simulation temperature used in ref 62.
(120) Hultman, L.; Barnett, S. A.; Sundgren, J. E.; Greene, J. E. Growth of epitaxial TiN films deposited on MgO(100) by reactive magnetron sputtering: the role of low-energy ion irradiation during deposition. *J. Cryst. Growth* **1988**, *92*, 639−656.
(121) Hultman, L. Thermal stability of nitride thin films. *Vacuum* **2000**, *57*, 1−30.

DOI: 10.1021/acs.jpcc.6b02652
J. Phys. Chem. C 2016, 120, 12503−12516

(122) Du, Y. G.; Dohnalek, Z.; Lyubinetsky, I. Transient mobility of oxygen adatoms upon O_2 dissociation on reduced TiO_2(110). *J. Phys. Chem. C* **2008**, *112*, 2649−2653.
(123) Note that the relatively ease of N−N bond breakage in N_2 gas molecules may be an artifact caused by the use of canonical NVT sampling of configurational space.
(124) Shin, C. S.; Gall, D.; Kim, Y. W.; Hellgren, N.; Petrov, I.; Greene, J. E. Development of preferred orientation in polycrystalline NaCl-structure δ-TaN layers grown by reactive magnetron sputtering: Role of low-energy ion surface interactions. *J. Appl. Phys.* **2002**, *92*, 5084−5093.

DOI: 10.1021/acs.jpcc.6b02652
J. Phys. Chem. C 2016, 120, 12503−12516